Investigation of Off-axis Excitation due to Component Asymmetry with a Non-Resonant Dynamic Stiffness Test Method

Undergraduate Honors Thesis

Presented in Partial Fulfillment of the Requirements for

Graduation with Distinction in the

Department of Mechanical Engineering at

The Ohio State University

By:

Adam C. Miller

Advisor: Dr. Rajendra Singh

Co-Advisor: Dr. Jason Dreyer

****

The Ohio State University

May 2012

Defense Committee:

Dr. Rajendra Singh

Dr. Jason Dreyer

Dr. Blaine Lilly

Abstract

Elastomeric bushings are common components in automotive vehicle suspensions and steering systems. They influence the vehicle noise and vibration as well as the handling performance by providing compliance to accommodate for misalignments and structural isolation at the joints of various linkages and frames. Dynamic properties of bushings are often measured using an elastomer test machine, in which the bushing is mounted into a fixture that mates to a displacement actuator on an upper crosshead and a force sensor on a lower crosshead. Typical elastomer test machines only actuate and record displacements and forces along a single axis. Possible misalignments of the mounting fixture or asymmetrical geometry of the bushings can induce off-axis motions and forces. To help illustrate and analyze this problem, a reference component with well known properties is developed and tested using the elastomer test machine. An analytical model of the reference component is developed to understand its behavior and interaction with the test machine dynamics. Modifications to the fixture setup are also analytically and experimentally investigated. Using results from this preliminary investigation, a refined reference component is suggested.

Table of Contents

Acknowledgements

I would like to thank all the people that have provided help and support over the course of this project. I am thankful for the guidance offered by both Dr. Rajendra Singh and Dr. Jason Dreyer, and the efforts of Dr. Blaine Lilly to critique my work and serve on my defense committee. I would also like to thank all the students and resources in the Acoustics and Dynamics Laboratory at The Ohio State University. This project would not have been possible without the facilities provided by the Department of Mechanical and Aerospace Engineering throughout Scott Lab. I would also like to acknowledge the National Science Foundation I/UCRC in Smart Vehicle Concepts at The Ohio State University for partial support of this project. Finally, a special thanks to Honda R&D Americas and YUSA Corp. for use of their commercial elastomer test systems as well as test support.

Table of Figures

Chapter 1: Introduction

1.1 Background

A typical radial bushing is illustrated in Figure 1.1. The bushing is comprised of an elastomeric material held between two hollow metal sleeves. This type of elastomeric bushing is commonly found in automotive suspensions. It is used to reduce vibrations and allow for misalignments in suspension components, such as trailing arms. The stiffness characteristics of the bushings have an influence on the handling and smoothness of a vehicle. Stiffer bushings are typically used for firmer, better handling suspensions, while less stiff bushings are used in softer, more forgiving suspensions. The outer sleeve is often fixed or constrained within a frame or linkage, while the inner sleeve is subjected to a displacement or force input from another frame or linkage. Depending on the nature of the load or displacement vector, the bushing can be subjected to a combination of moments and forces. A concept of a stiffness matrix is required to describe the reaction of the bushing within the system.

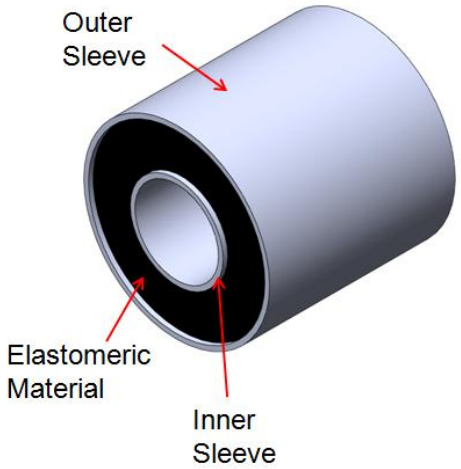

Figure 1.1: Schematic of typical elastomeric bushing.

Since bushings have a major impact on the handling and ride quality of a vehicle, it is very important to understand the dynamic properties of these bushings. One method of doing this is to employ an elastomer testing machine. Elastomer testing machines are used to dynamically characterize elastomeric materials. Values of the material, such as the dynamic stiffness, damping, and energy can be recorded. The specific machine being used for this experiment, the MTS 831.50, has a motion actuating upper crosshead and a force measuring lower crosshead.

Fixtures are needed to properly mount bushings to the upper and lower crossheads of the testing machine. These fixtures are typically designed with careful consideration to its stiffness and resonant frequencies so as to not influence the final results. A typical fixture for a radial bushing is shown in Figure 1.2; it consists of a lower fixture, such as a collar around the outside of the bushing that connects the bushing to the lower crosshead and an upper fixture, a fork that connects the upper crosshead and a bolt that passes through the center of the bushing.

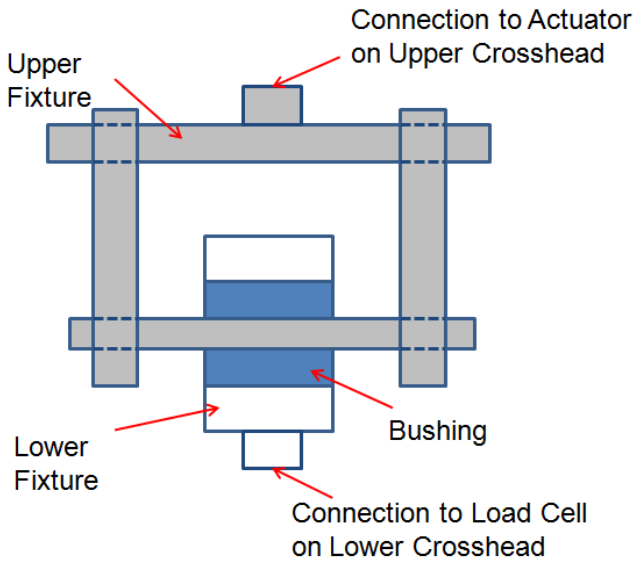

Figure 1.2: Typical fixture for radial characterization of cylindrical bushings in a single-axis elastomer test machine.

1.2 Literature Survey

Static and dynamic bushing properties are dependent on geometry, loading, material, manufacturing / assembly properties, and lead to nonlinear phenomena, such as hysteresis, rate and amplitude dependence, etc. Both frequency and time domain characterization of the stiffness and damping elements, including amplitude-sensitive and frequency-dependent properties are required to predict behavior of bushing components within systems. Estimation of the dynamic properties, such as force transmissibility or stiffness, of elastomeric bushings typically follows two approaches. In the first approach, the displacement- and rate-dependent material properties are estimated by curve-fitting parametric constitutive models to material testing data. These constitutive equations are then used in a finite element model to estimate the behavior of the bushing component under specific loading and boundary conditions. The behavior from these models is used to estimate the time dependent or frequency dependent behavior of the component. In the second approach, the component is characterized under controlled boundary and loading conditions. The behavior of these components is then represented as a combination of different viscoelastic elements, such as a Kelvin-Voigt, Maxwell, Standard Linear Solid, etc. Often separate models are required for either time (including transient analysis) or frequency domain behavior, respectively. Quantification of component dynamic properties can be done by either non-resonant or resonant testing, defined in Figure 1.3, although measured dynamic properties may vary among test methods. Multi-dimensional behavior, specifically coupling stiffness elements and their dependence on shapes and materials are not available or poorly understood. Moreover, test procedures for multi-dimensional property characterization are also sparse and often unverified. Dynamic stiffness

matrix elements are often reported as diagonal terms only since off-diagonal stiffness elements or coupling terms are difficult to directly measure or validate.

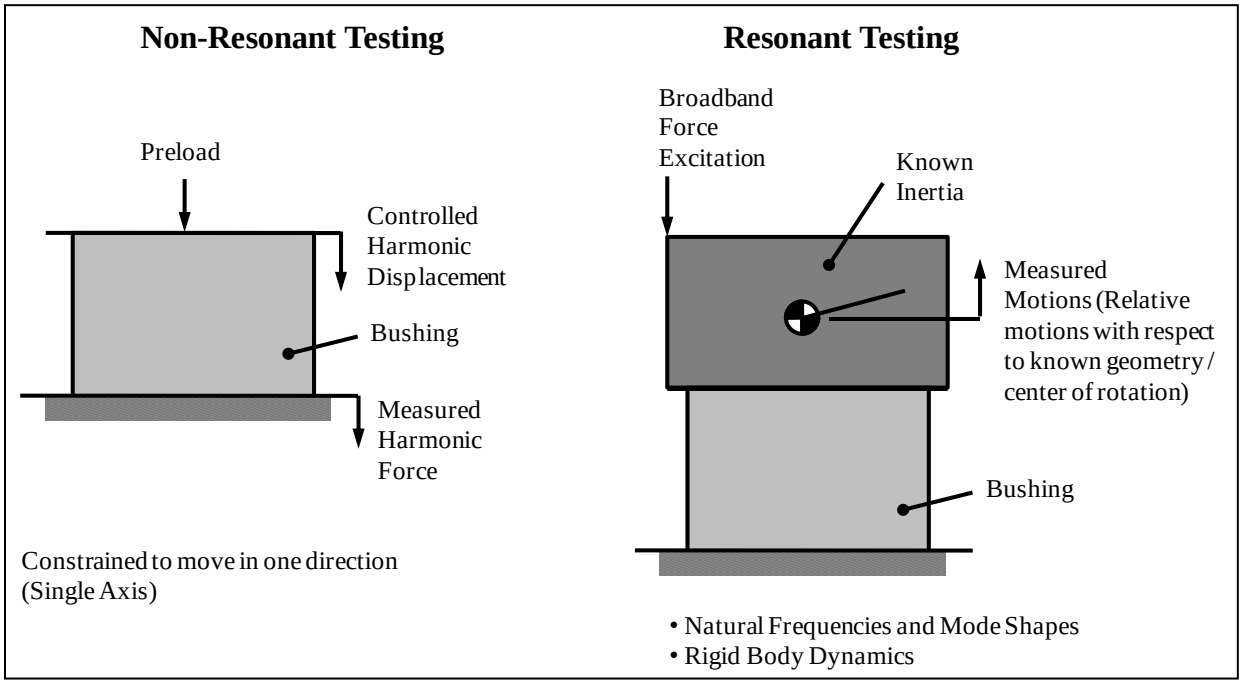

Figure 1.3: Quantification of component dynamic properties can be done by either non-resonant or resonant test methods. Measured dynamic properties may vary among test methods.

Although literature and methods on elastomeric component modeling and characterization are prevalent, specific applications to bushings are not as common. Some prior work has been done to define static stiffness terms of radial, axial, and torsional elements at given preload conditions in one or more directions (Barber, 1998; Garcia, 2006; Kadlowec et al., 2007; Senti et al., 2010); however, the coupling stiffness elements and their dependence on shapes and materials are not available or poorly understood. In order to characterize the dynamic properties of bushings, some works (Becker et al., 1999; Lee and Wineman, 1999; Kim and Singh, 2007; Taulbee, 2011) have employed simple lab experiments and techniques such as

frequency response, modal testing, and transfer path analysis; however, these results provide a "linearized" response which may not adequately describe the nonlinear nature of the components. There are a variety of computational methods for dynamic characterization of bushings referenced in literature (Gil-Negrete et al., 2007; Sohn et al., 2007; MSC Software, 2010), such as nonlinear finite element, multi-body dynamics, lumped parameter models, and empirical models; yet, these models often utilize minor or gross "adjustments" to fine-tune the system behavior, which implies a void in the state of the art. Some commercial experimental characterization methods for dynamic properties also exist. These methods often capture one type of force-deflection curve (such as axial or torsional) or certain elements of the stiffness matrix under sinusoidal testing (Barber, 1998; MSC Software, 2010). There have been some attempts to directly characterize the multi-dimensional properties of bushing components (Wolf et al., 2008); however, the addressing of boundary conditions and coupling elements in the stiffness matrices is still not resolved. Often the physical meaningfulness of these models and experimental results are unverified. In calculating the stiffness matrix of the system, there are an infinite number of different matrices that will produce the same behavior of any system; such models and methods do not determine or account for a unique solution to the stiffness of a particular system.

The focus of this project is to characterize fixture dynamics on a commercial elastomer test machine (non-resonant method) and investigate its effects on the dynamic measurements used in the stiffness calculation. The machine being used is the MTS 831.50 Elastomer Test System. This machine offers the ability to test elastomers up to a frequency of 1,000 Hz with a maximum force of ±10,000 N and a maximum dynamic displacement of ±25 mm at low frequencies (MTS Systems Corporation, 2011). The components are typically placed under a

preload condition, either in tension or compression, and controlled either as a mean load or mean displacement. After the component has equilibrated about this preload condition, the machine begins cycling at different crosshead displacements. As the machine cycles at the controlled sinusoidal displacements, the transmitted force is measured on the lower crosshead. The peak to peak amplitudes of the sinusoidal displacement and force time histories as well as the phase between the two waves are used to calculate the dynamic stiffness properties of the component (MTS Systems Corporation, 2000; Piersol and Paez, 2010). The concept is summarized in Figure 1.4.

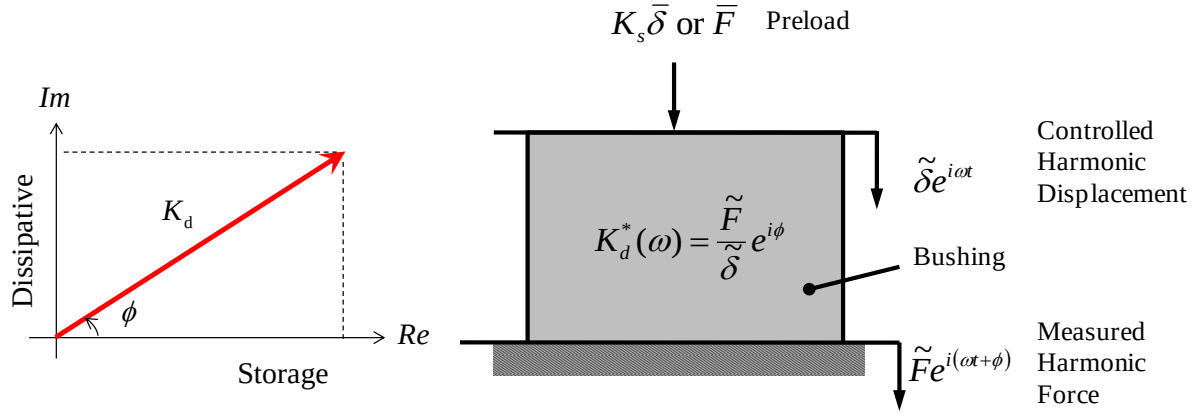

Figure 1.4: Schematic explaining complex stiffness estimation used by a non-resonant test method (MTS 831.50). Here $\tilde{F}$ is the harmonic force dynamic amplitude, $\tilde{\delta}$ is the harmonic displacement dynamic amplitude, $\bar{F}$ is the mean applied force, $\bar{\delta}$ is the mean applied displacement, ϕ is the phase shift between $\tilde{F}$ and $\tilde{\delta}$, K_d^* is the complex dynamic stiffness, K_s is the static stiffness, K_d is the dynamic stiffness magnitude, and ω is the harmonic excitation frequency.

The characterization conditions for a typical elastomeric bushing will include preloads up to +/-1000 N and peak-to-peak displacements of 3 mm. The static stiffness (0 Hz) of the hydro-bushing is approximately 500 N/mm. The dynamic stiffness of such bushings and mounts is typically greater than the static stiffness (depending on frequency), sometimes by a factor of 4 (Barszcz, 2010). Therefore, the maximum dynamic load that the fixture should be designed to withstand would be on the order of 6000 N peak-to-peak. Such a dynamic load would overcome the preload at certain frequencies causing the mount to be in both tension and compression over the course of a cycle. The frequency range required to characterize these bushings will be from 0 to 150 Hz. In order to accomplish this, the designed fixture should have its lowest resonance (in the actuation direction) above 200 Hz. This criterion will help ensure the excitation will only excite the stiffness controlled region of the fixture dynamics and therefore can be compensated for using the machine crosshead calibration procedure and a component with well-defined stiffness properties (Etapa, 2005).

1.3. Problem Formulation and Scope

The MTS 831.50 only measures forces in the vertical actuating direction; therefore elastomeric bushings properties can be characterized using the defined procedure, in one direction at a time. Features such as a wedged shaped bushing that will lead to off-axis bushing stiffness coupling is shown in Figure 1.5, resulting in a reaction moment. Inaccuracies locating the bushing in the test fixture can also result in a moment created during testing. These moments are not measured by the current machine and may have a significant impact on the output data. To compensate for this uneven loading within the machine, often pairs of components are tested together to react to each other and prevent moments from being generated. However,

misalignments are inevitable, and as will be shown as part of this thesis, even a minor misalignment can induce significant out of axis forces and out of plane moments. How these out of plane motions affect the measurement of the dynamic properties of the components are poorly understood. It is often heuristically approached by adjusting the test procedure until reasonable behavior (characteristic of an elastomeric component, outlined in previous section) is obtained. The proposed study will be restricted to a single plane, where the effect of an induced moment on the fixture / machine and its effect on measured dynamic properties of the component will be studied.

Specific objectives of this study include the following:

1) Design and testing of a reference component with well known properties to understand the effects of a moment on the measured and reported dynamic stiffness values from the elastomer testing machine
2) Development of an analytical model that can be used in conjunction the experimental data to determine the effective stiffness associated with the different boundary conditions.
3) Suggesting a reference component design that addresses some of the shortcomings of the current experiment for use on further research.

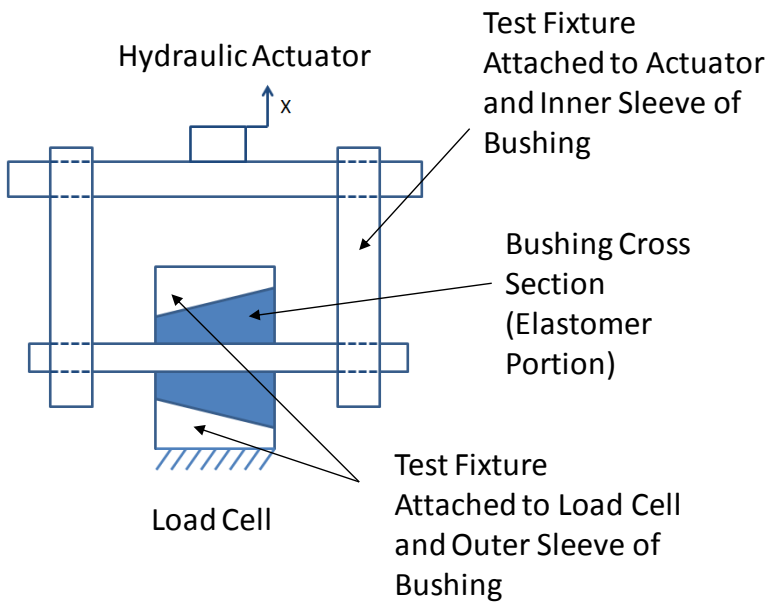

Figure 1.5: Typical Bushing with internal features that will induce out-of-axis motions into the test fixture / machine.

Chapter 2 will focus on the experimental component used for the two degree of freedom system. This chapter will include a discussion of the experimental setup, the methods and procedures for collecting data and a quick analysis of the effect of the moment on the recorded stiffness values. The experimental component will feature tension springs with known stiffness values so that experimental data may be compared to theoretical calculations. Chapter 3 will cover the derivation of an analytical model representing the experiment outlined in Chapter 2, and a comparison of the experimental and analytical systems will be presented. Chapter 4 addresses the design and construction of a reference component to be used for further research.

Chapter 2: Experimental Design to Investigate Cross-Coupling Due to Component Misalignment

2.1 Experimental Procedure

An experimental component was designed to be used on the MTS 831.50 Elastomer Test System. The component needed to be mounted in the machine and have known stiffness and geometric dimensions. Since it was assumed that any non-uniformity or misalignment of the bushing could lead to off axis motion that would create a moment in the system, it was important to design the fixture to investigate the effects of a moment. This was accomplished by creating a fixture that has both fixed and pinned end conditions. The main difference is that at the boundary where the fixture mounts to the machine the fixed case can support a moment while the pinned case cannot support a moment and is free to rotate. These end conditions are illustrated in Figure 2.1 (a) and (b), respectively.

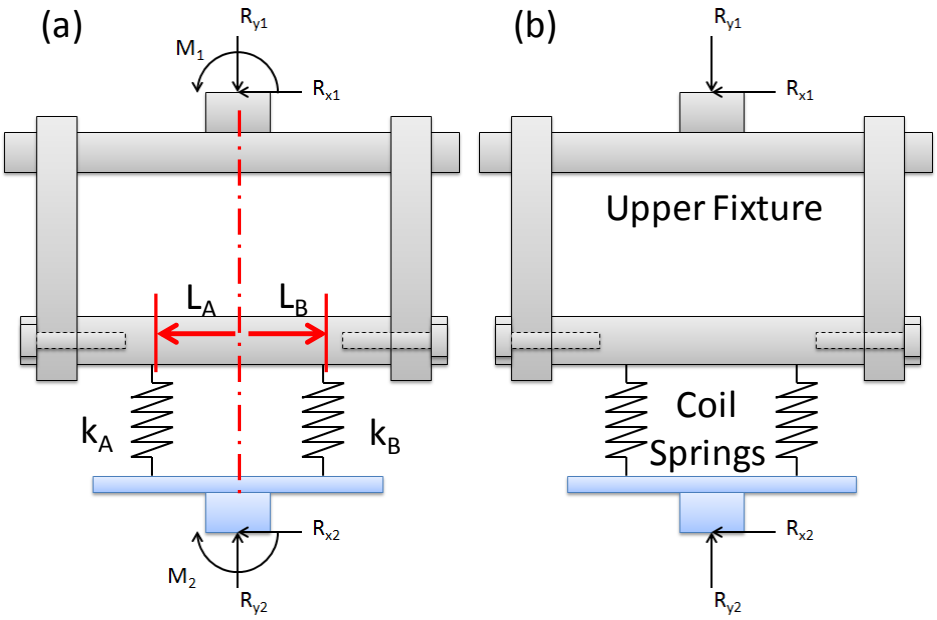

Figure 2.1: Schematics of initial investigation with component represented by the coil springs and fixture with (a) fixed and (b) pivoting attachments to the elastomer test machine. The vertical and horizontal reaction forces are represented as R_x and R_y, respectively, and the reaction moments are represented by M. The center distances of the springs, with respect to the central axis of the fixture are given by L, and the spring stiffnesses are given by k. Subscripts of 1 refer to upper fixture, subscripts of 2 refer to lower fixture, subscripts of A refer to left of center, and subscripts of B refer to right of center.

In addition to the end conditions it was also possible to change the spacing and stiffness of the springs being used. There were two different spring spacings used during the experiment, even and uneven. Even spring spacing resulted in both springs being centered 38.1 mm (1.5 inches) from the center line of the fixture, while uneven spacing consisted of one spring 38.1 mm (1.5 inches) and the other 25.4 mm (1 inch) from the center. A narrow even spacing, where both

springs are 1 inch from the center, was available but was not used for any of the tests. The two possible springs being used had stiffnesses of 17.9 N/mm (102 lbf/in) and 12.6 N/mm (72 lbf/in), as determined under static load conditions. Various combinations of the end conditions, spring spacing, and spring stiffness were tested. Table 2.1 shows the actual configurations that were used for each case.

Table 2.1: List of different test cases.

	Spring A (N/mm)	Spring B (N/mm)	Orientation	End Condition
Case 1	17.9	17.9	Even	Fixed
Case 2	17.9	17.9	Even	Pinned
Case 3	17.9	12.6	Even	Fixed
Case 4	17.9	12.6	Even	Pinned
Case 5	17.9	17.9	Uneven	Fixed
Case 6	17.9	17.9	Uneven	Pinned

The cases with fixed end conditions were tested first. To start each fixed case the springs were preloaded to the same initial displacement of 5 mm. This resulted in different preload forces when different springs were used. To keep the tests consistent between the fixed and pinned fixtures the preload force on the pinned fixture was matched to the preload force that was measured by the machine during the fixed case. A schematic of the test setup with nominal dimensions is given in Figure 2.2. The test being run by the MTS 831.50 consisted of a 1 mm peak to peak axial displacement across a frequency sweep of 1 to 100 Hz in 1 Hz increments. When the pinned fixture was tested it was noted that frequencies above 80 Hz started to excite a resonant frequency in the bolted connection, and the resulting data was unusable. As a result of this and in the interest of leaving the fixture unharmed all of the pinned cases were only tested to 80 Hz.

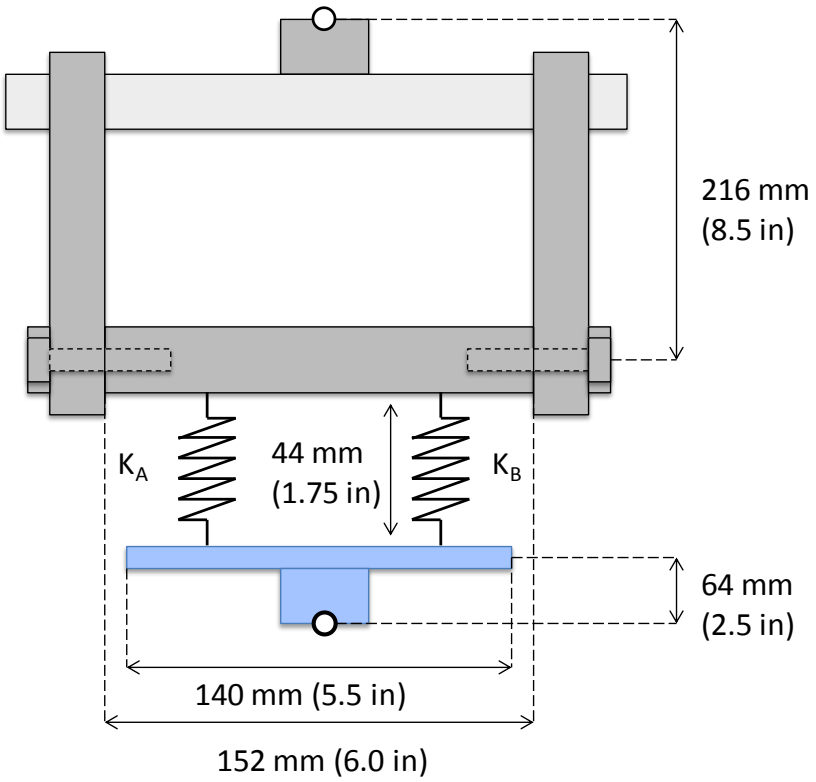

Figure 2.2: Schematic of test fixture setup with nominal dimensions.

2.2 Data Collection

Accelerometers are mounted in locations A1 and A2 as shown in Figure 2.3. Accelerometer 1 measures the off axis acceleration of the upper fixture in the x_1 direction while accelerometer 2 measures the off axis acceleration of the lower fixture in the x_2 direction. The uniaxial piezoelectric accelerometers (PCB model UJ352C66) used each had sensitivities of 100 mV/g and were run through a conditioner with a gain of 1 before being read by the auxiliary input on the MTS machine. The test specimen output file includes peak to peak amplitudes of the stiffness, measured axial force, axial displacement, and accelerations at each frequency tested.

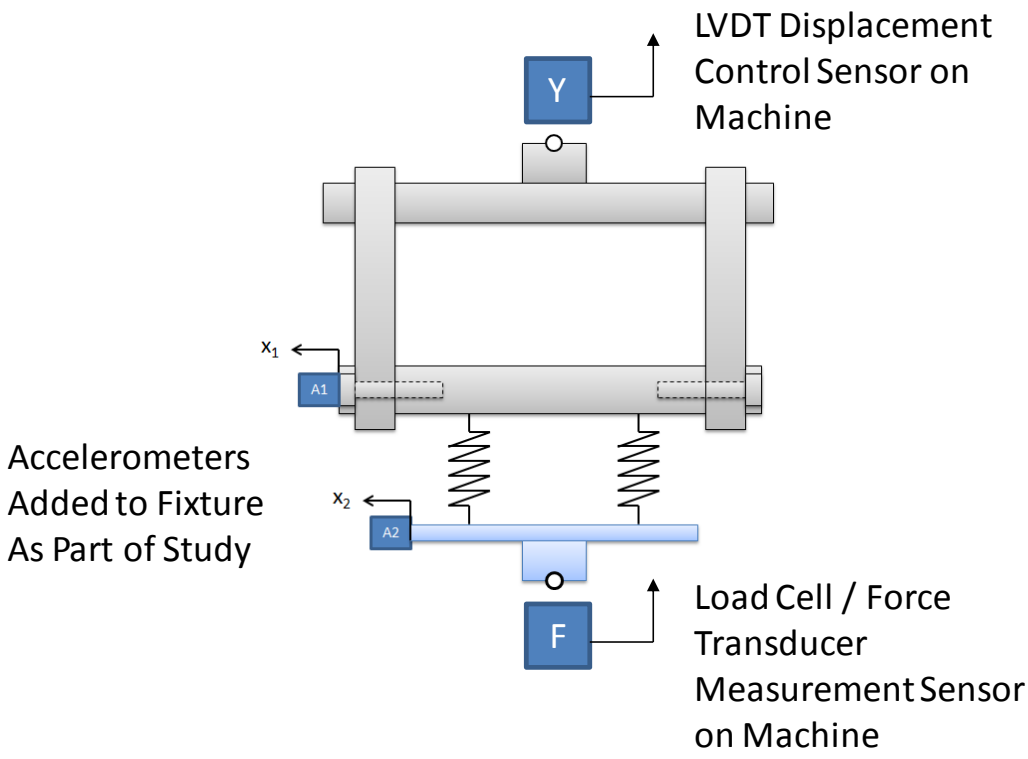

Figure 2.3: Locations of sensors in this study. Accelerometers are given by A1 and A2 for upper and lower fixture, respectively, oriented in horizontal (x) direction. The displacement control sensor on upper test machine crosshead is given by Y, and the load cell / force transducer on lower test machine crosshead is given by F, both measuring in the vertical (y) direction.

2.3 Effect on Stiffness and Acceleration

The dynamic stiffness of the component is determined using the displacement of the actuator and the force recorded through the force sensor mounted on the lower crosshead. Figure 2.4 below shows a comparison of the dynamic stiffness of the component as measured for the fixed and pinned cases when the springs were located in the even position. The actual stiffness of the springs was verified using a tensile test. The springs had a stiffness of 17.9 N/mm (102 lbf/in). It follows that the nominal static stiffness for this configuration with two springs in

parallel is 35.8 N/mm (204 lbf/in). Representative frequency dependent stiffness curves for the two fixtures are shown in Figure 2.4. Although there is a slight drift in the stiffness values as frequency increases, this is still within machine tolerances for mean and dynamic amplitudes set to 5%. As expected, the measured stiffness across the fixture using the linear variable differential transformer (LVDT) in the upper crosshead and force sensor in lower crosshead yields a frequency independent stiffness trend, expected for coil springs under relatively small deflection. At higher (past 150 Hz) frequencies, it was observed that the machine was having issues maintaining peak to peak displacement values, especially for configurations of springs that were non-symmetric about the central axis of the fixture. For the studies shown, only frequencies below 100 Hz will be used, for which the machine appeared to behave as expected (maintaining control parameter inputs).

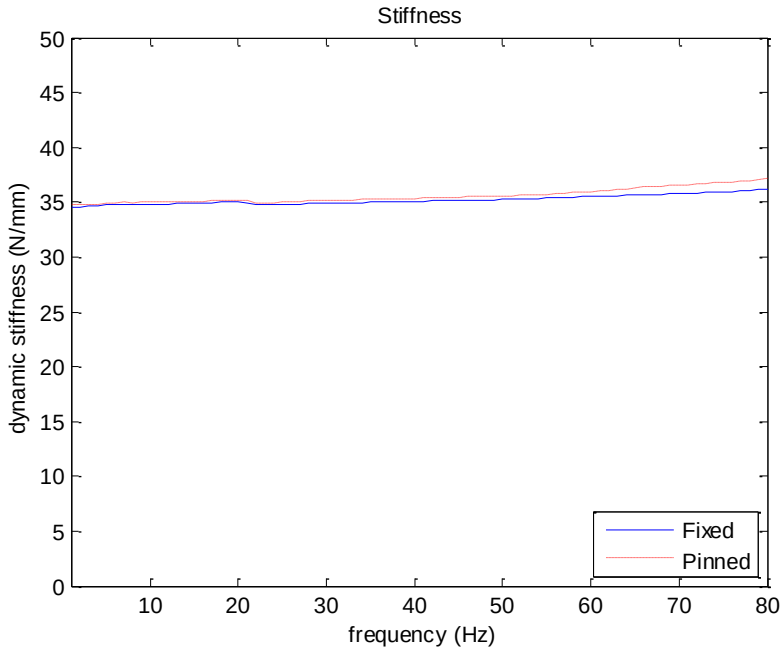

Figure 2.4: Calculated dynamic stiffness curve of component with 35.8 N/mm springs at 38.1 mm equal spacing from center of fixture.

Figure 2.5 shows all of the accelerometer data for the cases when the fixture is fixed. Figure 2.6 presents the same data when the fixture is pinned. The fixed cases all exhibit a peak around 74 Hz recorded by the top accelerometer; this same peak does not occur when the fixture is pinned. This observation seems to suggest that a moment or off-axis force in the system will excite a resonant frequency in the machine and induce off-axis motion. The resonant frequencies for all case can be seen in table 2.2.

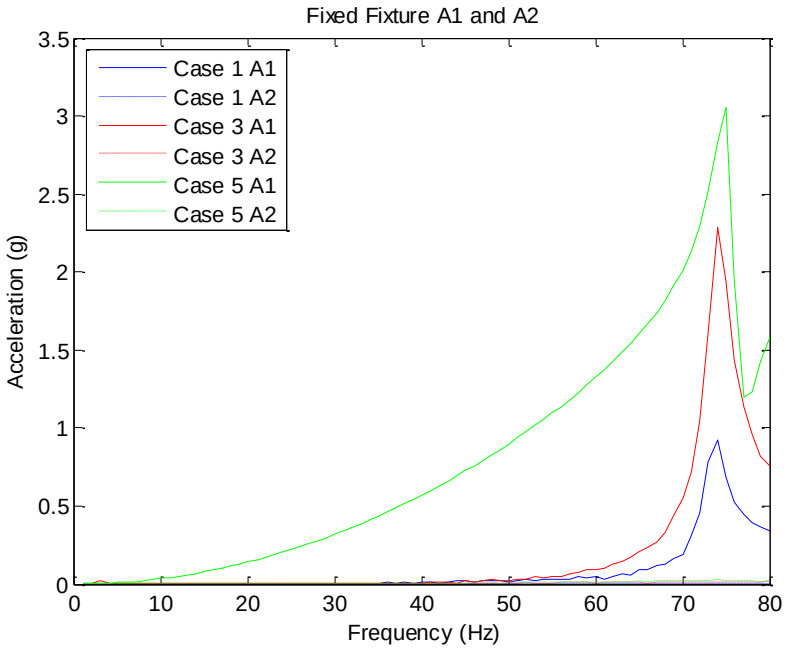

Figure 2.5: Measured accelerations from accelerometers A1 (solid lines) and A2 (dotted lines) for different fixed fixture test cases.

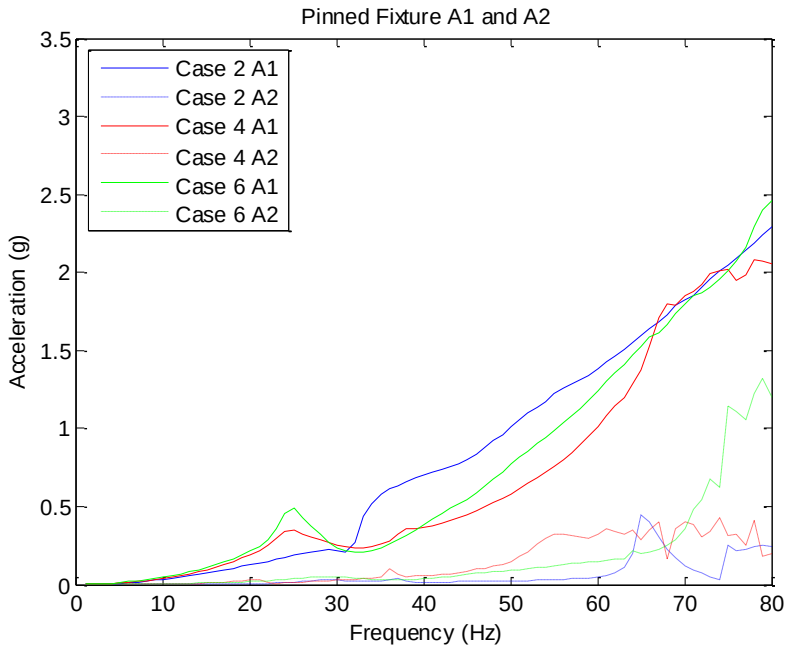

Figure 2.6: Measured accelerations from accelerometers A1 (solid lines) and A2 (dotted lines) for different pivoting fixture test cases.

Table 2.2: List of resonant frequencies for different test cases.

Case	Resonant Frequency (Hz)
1	75
2	31
3	74
4	25
5	74
6	25

Significant vibration response of the fixture in the off-axis direction is observed. Instead of the resonance peak at 74 Hz that was observed for the fixed case, the pinned case exhibits a peak around 25 Hz. An analytical model will be developed to help better understand the accelerometer data and explain this shift in resonances between cases.

Chapter 3: Proposed Simple Analytical Models of Experimental Setups

3.1 Derivation

An analytical model was developed from the proposed test fixture. This simple model includes only the two degrees of freedom (DOF) that exist in the test setup. The degrees of freedom are shown in Figure 3.1. The upper fork has a rotational degree of freedom due to the pinned connection or moment flexure in the fixed connection case as it is subjected to a vertical displacement at the base of the fixture attached to the upper actuator. The lower plate has a rotational DOF again due to its pinned connection or moment flexure in the fixed connection case. Since the displacement of the upper fixture is controlled by the testing machine, it will be treated similar to a base excitation imparting a moment through the springs A and B.

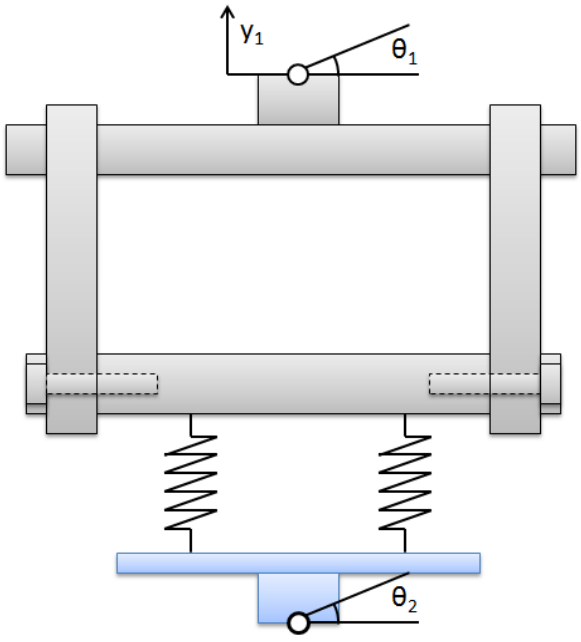

Figure 3.1: Actuation displacement (y_1) and rotation DOFs (θ_1 and θ_2) for upper and lower fixtures respectively.

The simplified test fixture schematic is shown in Figure 3.2. The inertia values are calculated using a solid model of the fixture rotating about the points O_1 and O_2 for the upper and lower crossheads, respectively. These beams are connected to each other through two springs that have stiffnesses of K_A and K_B and are located a distance, L_A and L_B, from the center of the fixture. The model is excited by a controlled displacement acting on beam 1 at its center of mass in the y_1 direction. The rotation of beams 1 and 2 is restricted by torsion springs acting at the center of mass of each beam, the stiffness of the springs are K_{T1} and K_{T2}, respectively.

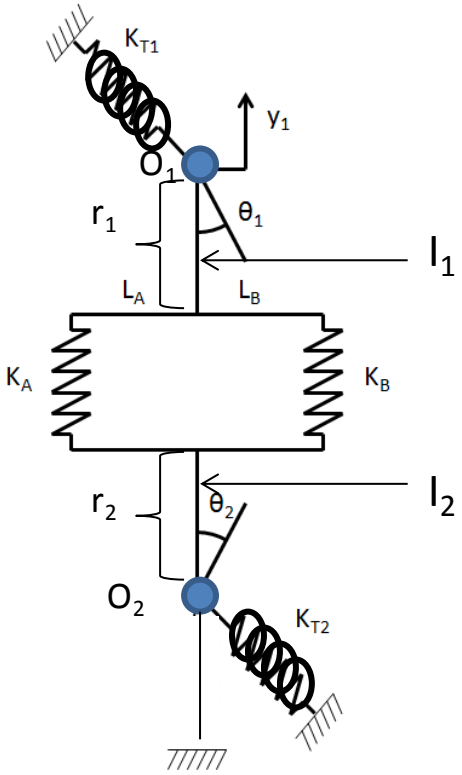

Figure 3.2: Schematic of mechanical elements (inertia *I*, coil spring stiffnesses *K*, torsional spring stiffnesses associated with fixture constraints K_T), dimensions *r* and *L*, and degrees of freedom θ, and displacement excitation *y*. The subscript of 1 refers to lower fixture, subscript of 2 refers to upper fixture, subscripts A and B refers to left and right side of central axis of fixture (determined by the connection of points O_1 and O_2).

Figure 3.3 shows the free body diagram of the upper fixture where y_1 is the displacement of the upper actuator on the fixture as a result of the machine's controlled sinusoidal displacement. F_A and F_B are the forces due to springs A and B located L_A and L_B from the center of the fixture. The rotational equation of motion taken about point O_1 can be derived by inspection from the free body diagram and is shown as the equation below.

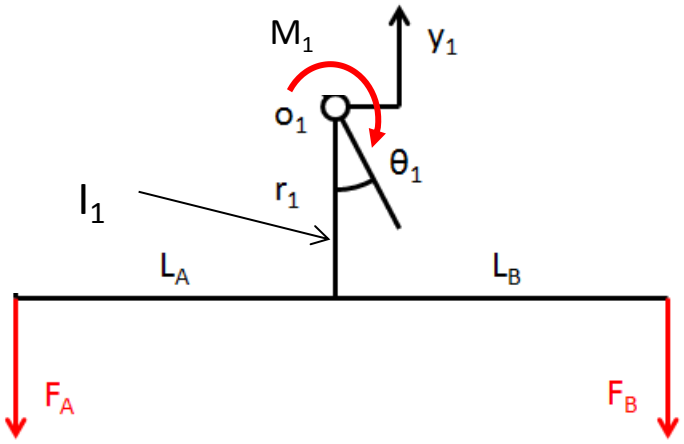

Figure 3.3: Free body diagram of upper fixture with reaction moments M and forces F due to the torsional spring and coil springs, respectively.

$$I_1\ddot{\theta}_1 = L_A F_A - L_B F_B - K_{T1}\theta_1 \qquad (1)$$

The free body diagram for the lower fixture is shown in Figure 3.4. The equation of motion about O_2 is found similarly to upper fixture and is written as the equation below.

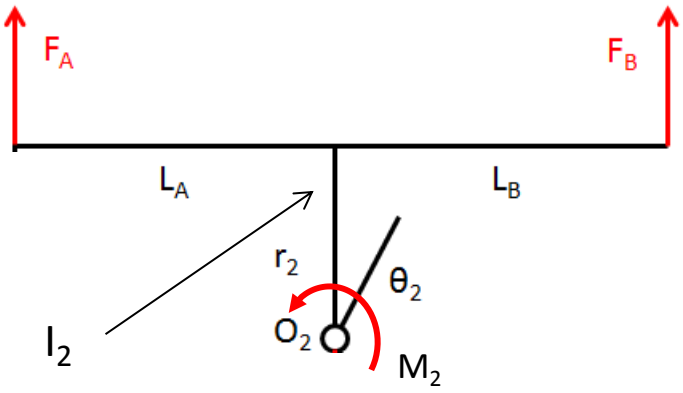

Figure 3.4: Free body diagram of lower fixture with reaction moments M and forces F due to the torsional spring and coil springs, respectively.

$$I_2\ddot{\theta}_2 = L_A F_A - L_B F_B - K_{T2}\theta_2 \qquad (2)$$

The accelerations of the test component were measured in the x_1 and x_2 directions according to Figure 2.2. A simple geometric transformation can be used to write the equations of motion in terms of x_1 and x_2 instead of θ_1 and θ_2, where r_1 and r_2 are the vertical distances from the pin to the accelerometers for the upper and lower fixtures, respectively.

$$x_1 = \theta_1 r_1 \qquad (3a)$$

$$x_2 = \theta_2 r_2 \qquad (3b)$$

F_A and F_B can be determined as functions of the motion of the two fixtures, and the stiffnesses and locations of the springs.

$$F_A = K_A\left(y_1 - L_A\theta_1 - L_A\theta_s\right) \qquad (4a)$$

$$F_B = K_B\left(y_1 + L_B\theta_1 + L_B\theta_s\right) \qquad (4b)$$

Rearranging these equations in the frequency domain results in the following matrices that govern the motion of the system, assuming single frequency sinusoidal excitation:

$$\begin{bmatrix} \left(-\omega^2 I_1 + K_A L_A^2 + K_B L_B^2 + K_{T1}\right)/r_1 & \left(K_A L_A^2 + K_B L_B^2\right)/r_2 \\ \left(K_A L_A^2 + K_B L_B^2\right)/r_1 & \left(-\omega^2 I_2 + K_A L_A^2 + K_B L_B^2 + K_{T2}\right)/r_2 \end{bmatrix} \begin{bmatrix} x_1 \\ x_2 \end{bmatrix} = \ldots$$

$$\ldots = \begin{bmatrix} y_1\left(K_A L_A - K_B L_B\right) \\ y_1\left(K_A L_A - K_B L_B\right) \end{bmatrix} \tag{5}$$

When attempting to match the analytical prediction to the experimental results it was noticed that the amplitude of resonant frequency of the analytical model was reaching unrealistically large values. To correct this, a torsional damping element (viscous in nature) was added to each of the fixtures. This is shown in Figure 3.5.

$$\begin{bmatrix} \left(-\omega^2 I_1 + j\omega C_{T1} + K_A L_A^2 + K_B L_B^2 + K_{T1}\right)/r_1 & \left(K_A L_A^2 + K_B L_B^2\right)/r_2 \\ \left(K_A L_A^2 + K_B L_B^2\right)/r_1 & \left(-\omega^2 I_2 + j\omega C_{T2} + K_A L_A^2 + K_B L_B^2 + K_{T2}\right)/r_2 \end{bmatrix} \begin{bmatrix} x_1 \\ x_2 \end{bmatrix} = \ldots$$

$$\ldots = \begin{bmatrix} y_1\left(K_A L_A - K_B L_B\right) \\ y_1\left(K_A L_A - K_B L_B\right) \end{bmatrix} \tag{6}$$

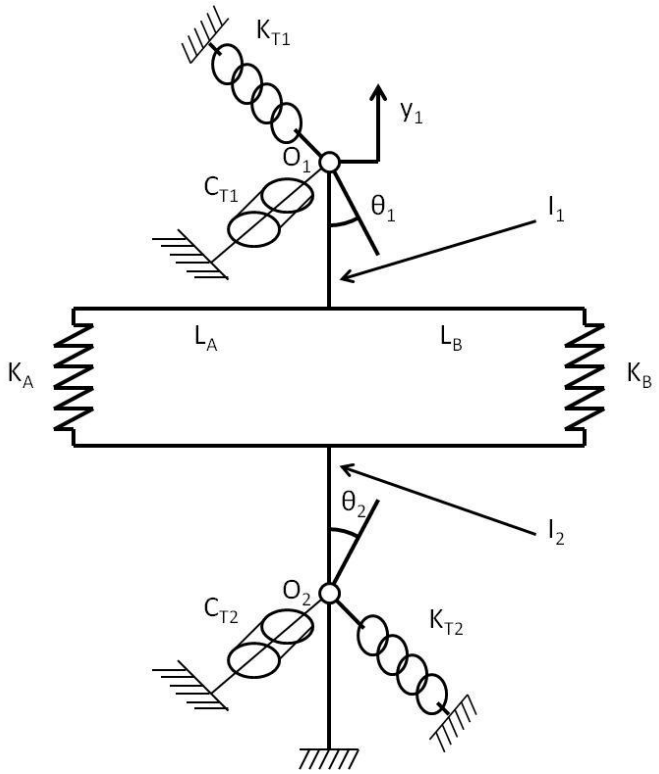

Figure 3.5: Extension of Figure 3.2 with torsional damping C_T at points O_1 and O_2

The mass and inertia of the two beams was determined from the solid models shown in Figures 3.5(a) and (b) using measured geometries and assumed material properties. The figures depict the location of the pinned connections as well as each fixture's center of mass. The moment of inertia about the pinned connections was calculated using the parallel axis theorem. The values used in the final analysis are located in Table 3.1.

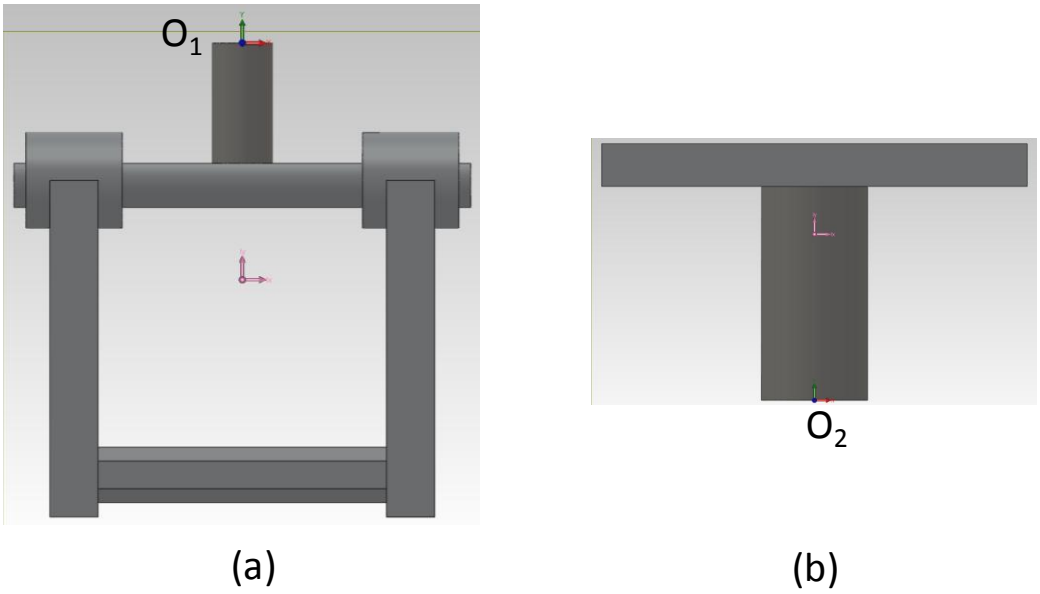

Figure 3.6: Solid models of the (a) upper and (b) lower fixture used to estimate inertial properties. Properties taken about point O_1 for upper fixture and point O_2 for lower fixture.

Table 3.1: Mass properties for Upper and Lower Fixture, where y_c is the distance from pivot location O to the center of mass of the fixture component, I_o is mass moment of inertia of the fixture component about it center of mass, I is the mass moment of inertia of the fixture component about it pivot point.

Fixture	mass (kg)	y_c (m)	I_o (kg*m^2)	I (kg*m^2)
Upper (subscript 1)	2.46	-0.125	0.0268	0.06524
Lower (subscript 2)	0.72	0.0493	0.0009	0.00265

3.2 Determination of Torsional Stiffness

To fit the analytical model to the experimental data, the nominal values of K_A, K_B, L_A, and L_B, the computed values for I_1 and I_2, and the measured values of y_1 and ω were used. The torsional stiffness K_T of the upper and lower fixtures was found graphically from experimental data by varying the stiffness until the resonance frequency of the analytical model matched the frequency observed in the experimental data. This occurred at a representative value of 15000 N-m/rad for the fixed fixture and an order of magnitude lower (1500 N-m/rad) for the pinned fixture. For both fixtures, an addition of damping values C_{T1} and C_{T2} of up to 1 N-m/rad/s was required to realistically fit the amplitudes of the measured accelerations. Physically, this damping would correspond to damping seen within the load frame and actuator. Ideally the torsional stiffness at the pinned joint would be zero; however due to the inherent friction within the joint under preload, a nominal torsional stiffness was considered. The experimental setup with a pivoting joint was used primarily as a comparison of results to a different boundary condition of the fixture, as it quickly became a difficult physics to capture. An improved dry friction model may better explain this result as well as better correlate the two experiments.

In addition, a component of the vertical acceleration of the cross head in the y_1 direction was observed in the upper fixture acceleration measurement in the x_1 direction (accelerometer A1). Cross axis sensitivity due to the axial misaligned position of the fixture within the machine as well as mounting of the accelerometer to the fixture would cause such a result. Therefore, a correction factor α was also used to adjust for this vertical component on the upper fixture accelerometer. The calculated value for acceleration of upper fixture based on Equations (5) for the fixed fixture and (6) for the pivoting fixture added to the calculated acceleration of the upper crosshead, based on the displacement y_1 , i.e. $-\alpha\omega^2 y_1$ was added to this acceleration $-\omega^2 x_1$. A

value of α = 0.18 was selected based on the best agreement with the magnitudes of the analytical data and experimental data for all cases and was kept the same for each case. Figures 3.7 and 3.8 show the comparison of the analytical model and experimental data for Case 5, representative for the fixed fixture conditions, and for Case 6, representative for the pivoting fixture conditions, respectively. Values used in the simulation are shown in table 3.2. An explicit expression for the accelerations at point A1 and A2 can be determined via Cramer's rule.

Table 3.2: Parameters of Analytical Model

	Fixed	Pinned
y_1 (mm)	0.5	0.5
L_A (mm)	25.4	25.4
L_B (mm)	38.1	38.1
K_A (N/mm)	19	19
K_B (N/mm)	19	19
r_1 (mm)	215.9	215.9
r_2 (mm)	63.5	63.5
I_1 (kg*m^2)	0.06524	0.06524
I_2 (kg*m^2)	0.00265	0.00265
K_{T1} (N/mm)	15	1.5
K_{T2} (N/mm)	15	1.5
C_{T1} (N-m/rad/s)	1	1
C_{T2} (N-m/rad/s)	1	1
α	0.18	0.18

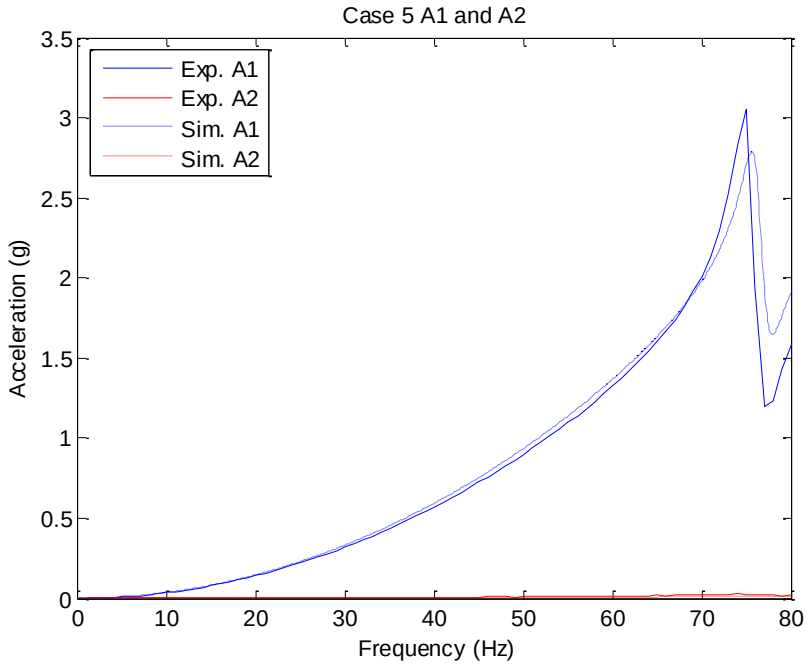

Figures 3.7: Comparison of the analytical model and experimental data for Case 5 (fixed fixture condition) for accelerometers A1 and A2.

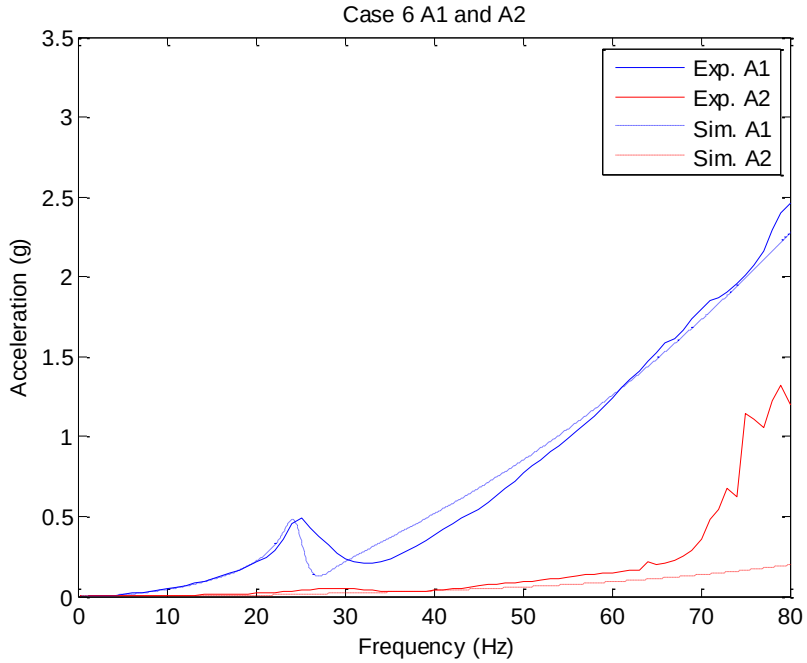

Figures 3.8: Comparison of the analytical model and experimental data for Case 6 (fixed fixture condition) for accelerometers A1 and A2

For both boundary conditions the resonance peaks of accelerometer 1 occur at values determined by equation (7). This indicates that the inertia of the beams and torsional stiffnesses are the most sensitive variables in determining the resonance frequency of the system. Therefore the accuracy of the graphically determined K_T depends heavily on the accuracy of the calculated inertia values.

$$\omega_n = \frac{1}{2\pi}\sqrt{\frac{K_{T1}}{I_1}} \qquad \text{Hz} \qquad (7)$$

Chapter 4: Design Considerations and Suggested Improvements of a Bushing Reference Component

One problem observed during testing of the two spring reference component is that preloading the system resulted in a rotation of the upper and lower fixtures in order for them to achieve static equilibrium. This rotation directly affects the acceleration measurements. In order to compensate for this issue a reference component that can be preloaded before being mounted in the elastomer testing machine will be designed. The new component will add an additional pair of springs opposite the existing springs so that the displacement of each spring pair will be the same. A drawing of the proposed component can be seen in Figure 4.1.

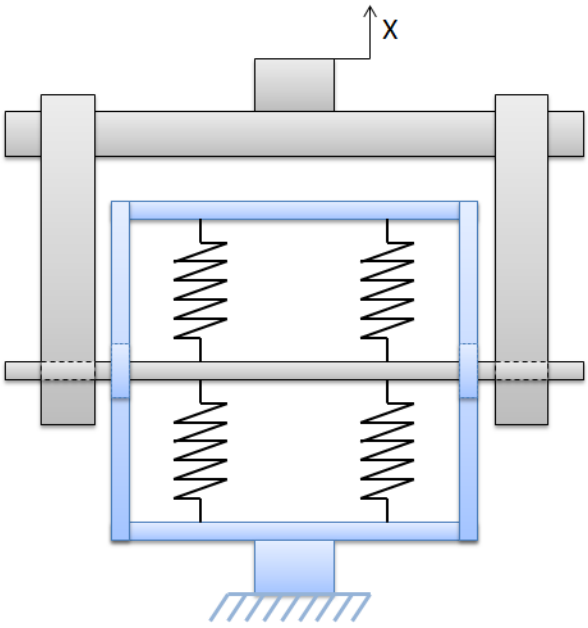

Figure 4.1: Schematic of improved reference component, more representative of a bushing component.

This new component requires a more complicated lower fixture. The lower fixture must have two parallel plates instead of one for connecting the springs; it must be possible adjust the

distance between the plates in order to preload the springs, and the lowest resonant frequency of the frame must be high enough to not influence the test data. The solid model of the design is shown in Figure 4.2. The springs will be connected to the parallel plates using eyebolts in the same manner that they were used for the two spring component. The four vertical rods in the figure represent all threads and will be used along with nuts to keep the parallel plates in place during testing. Lock washers will be used to prevent the nuts from becoming loose due to vibrations. The bottom plate has the same dimensions as the two spring component and will be mounted to the machine in the same manner.

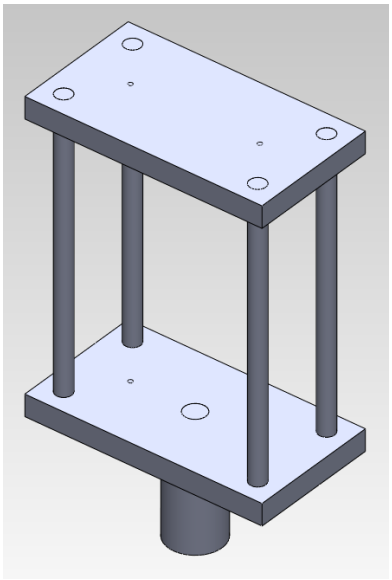

Figure 4.2: Solid model of proposed reference bushing design.

To ensure that the fixture is sufficiently stiff so as to not influence the testing data a simulated natural frequency analysis will be used. The cage is constrained in all degrees of freedom along the bottom face of the cylindrical rod, simulating the connection to the testing machine at the same location. Two spring connections are made between the upper and lower plates, and both springs have a stiffness of 17.5 N/mm (100 lbf/in) and a preload in tension of

44.5 N (10 lbf). The constraint and spring connections can be seen in Figure 4.3. The first five natural frequencies are presented in Table 4.1, and the displaced structure corresponding to the lowest natural frequency is shown in Figure 4.4.

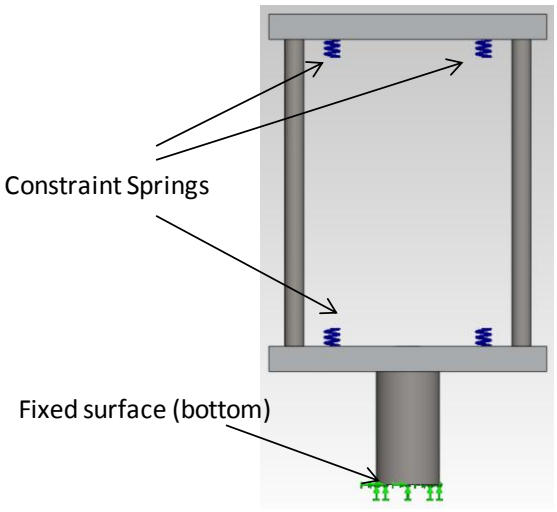

Figure 4.3: Solid model of proposed reference bushing design, with constraint springs and fixed base. These are the representative boundary conditions used for finite element analysis.

Table 4.1 Natural Frequencies of the Proposed Fixture Setup with Boundary Conditions Given in Figure 4.3.

Number #	Frequency(Hz)
1	167.2
2	168.0
3	294.9
4	980.1
5	1017.0

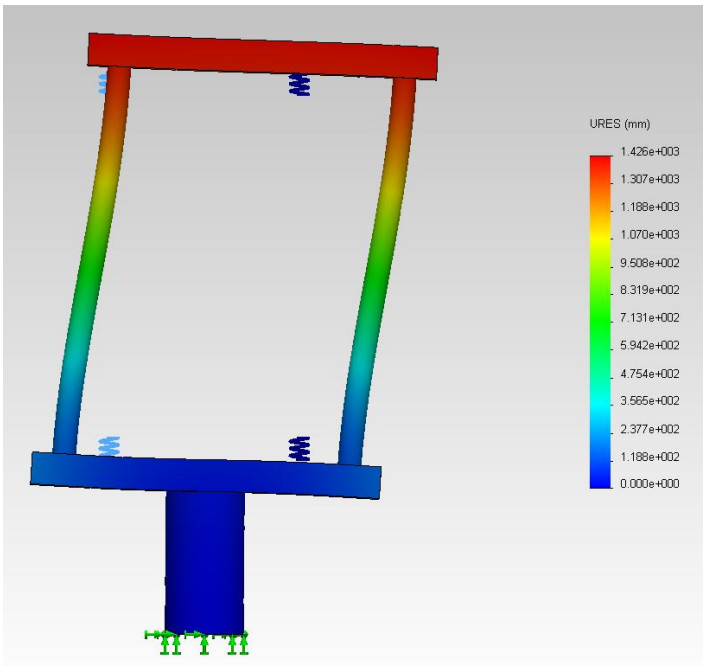

Figure 4.4: Deformed view of the mode shape corresponding to first (lowest) natural frequency

The lowest natural frequency of the frame occurs at 167 Hz. The mode shape corresponding to this frequency acts along the same plane that acceleration data was collected. Therefore, it would be expected that if the frame was actuated at 167 Hz by the testing machine that a resonance peak due to the frame would be noticeable in the acceleration data. Any induced motion in an out of plane direction due to a resonance may also amplify any coupling effects that the test component may be sensitive to. The resonance frequency of the frame is large enough that the dynamics of the frame would not be expected to influence the acceleration data if the original experiment were repeated, from 1 to 100 Hz. A physical prototype has been constructed, though it has yet to be tested or validated.

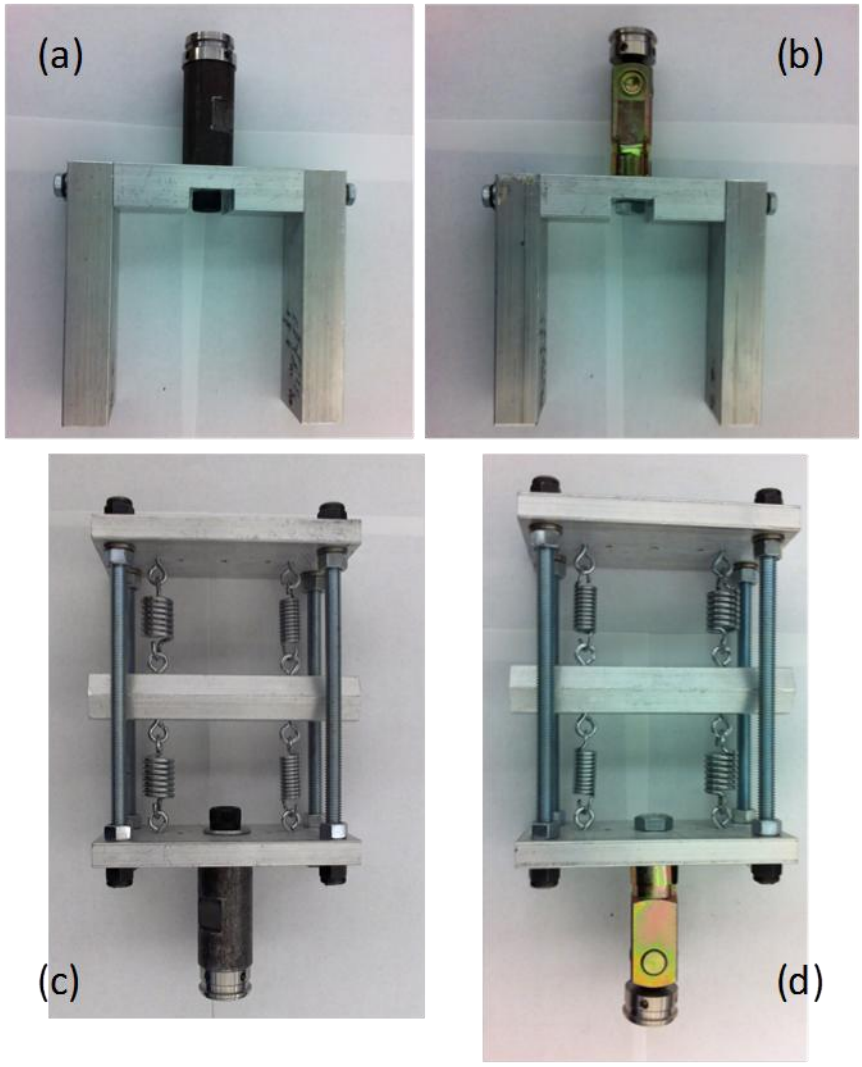

Figure 4.5: Physical prototype of bushing fixture concept for (a) upper fixture – fixed condition, (b) upper fixture – pinned condition, (c) lower fixture – fixed condition, and (d) lower fixture – pinned condition

Chapter 5: Conclusion

5.1 Conclusions

An experiment was designed with well known properties and tested to determine the effects of a moment induced, from asymmetry in the bushing loading conditions, on the measured and reported dynamic values from the elastomer test machine. An analytical model was derived to describe the experiment and used to determine the torsional stiffness associated with the boundary conditions. This model has the potential to use additional measurement data on the machine (such as out-of-axis accelerations) to estimate coupling parameters in a stiffness matrix of the experiment. Based on this study, a reference component was designed and built to address some of the observed shortcomings in the current experiment.

The experimental setup showed very little change in the measured stiffness of the component between the fixed and pinned cases. This can be explained by the fact that the springs of the experimental component were only acting in the vertical direction. Had an actual bushing with stiffnesses in all six degrees of freedom been tested it cannot be assumed that the reported stiffnesses would have remained as close. Changing the end conditions did however result in a noticeable difference in the acceleration data. A change in resonance frequencies occurred as a result of changing from fixed to pinned end conditions.

The analytical model provided an explanation for the change in resonance frequencies that was observed in the experimental data. The model was adjusted to match the magnitude and resonance frequency of the acceleration measured at accelerometer one; this resulted in accelerations at accelerometer two that were close in magnitude to experimental data but did not closely match the trend of the experimental data. This procedure serves as a method for

determining the torsional stiffness due to the boundary conditions acting on the fixtures. This information can eventually be used to refine test procedures, fixtures, and setups to better determine dynamic properties of components.

The main source of error during the experiment arose from the fact that the reference component needed to be preloaded in the test machine so that the springs would remain in tension during the entire test. When the pinned component was preloaded a rotation of the fixtures could be observed prior to any frequency testing. This resulted in a component of the vertical acceleration due to the machine being recorded by accelerometers as the accelerometers were no longer perfectly oriented in the horizontal direction. It is unclear how great of an impact this had on the results; however, a new reference component was designed to address this issue, as it can be preloaded separate from the machine and without rotating.

5.2 Recommendations for Future Work

Future work can be conducted to expand upon the concepts of this research. The reference component used during this experiment made two important simplifications. First, the component was developed to only have a two dimensional stiffness matrix, consisting of translational and rotational stiffness elements along with the coupling terms. The second simplification was that since steel tension springs were used to construct the component, it was assumed that there was no damping in the component. Expanding this research to include more degrees of freedom, resulting in larger stiffness matrices and materials that will provide damping in the component is necessary in order to eventually be able to predict the behavior of an elastomeric bushing with six degrees of freedom.

The proposed analytical model for the original component correlates well with experimental data. However, the fixture and machine specific damping and stiffness parameters

are empirically estimated. Adding the pivot joint in the fixture in order to decouple the bushing system from the machine dynamics due to an induced moment did not yield expected results, as the pivot joint did not fully decouple the bushing component from the machine dynamics. It was also observed to cause more variability at higher frequencies as sufficient effective forces and moments were generated to drive the system between different stiffness regimes due to clearances in out of plane directions in the joint. Regardless of the limitations in decoupling the bushing system from the machine dynamics, a method to determine the two-dimensional stiffness matrix from experimental data could be developed if the machine stiffness and damping parameters are well understood. The method would solve for the stiffness and center position of the springs using the analytical model and the experimental displacement and accelerations.

Further research can be conducted with the new reference component to verify the observations based on the stiffness and motion data. The new component should provide a way to more accurately measure the rotation of the fixture without the error discussed earlier. The pivot joint would most likely be replaced with some sort of spherical joint to better decouple the fixture from the machine, and a characterization procedure would have to be developed to determine the machine stiffness and damping parameters in out of plane directions (not in actuation direction). Further work may be required to successfully represent the new component with an analytical model. The results of this work can also be compared to resonant techniques that have shown potential in estimating elements of the multi-dimensional stiffness matrix of a component. The main advantage of adapting a commercial test machine and a non-resonant method to extract these parameters is the ability to preload the component and excite it with higher displacement amplitudes, often not possible using linear system (modal) techniques.

References

Barber, A. J. "Accurate Models for Bushings and Dampers Using the Empirical Dynamics Method," MTS Technical Paper, 1-29, 1998.

Barszcz, B, *Dynamic Tuning of Hydraulic Engine Mount Using Multiple Inertia Tracks*, Masters Thesis, The Ohio State University, 2010.

Becker, P., R. Wynn Jr., E. Berger, and J. Blough. "Using Rigid-Body Dynamics to Measure Joint Stiffness" *Mechanical Systems and Signal Processing* (1999): 13(5), 789-801.

Etapa, J.C., *High Frequency - Low Amplitude Dynamic Characterization of Elastomers through Experimental Techniques*, Master's Thesis, Michigan Technological University, 2005.

Garcia, M.-J. "Engineering Rubber Bushing Stiffness Formulas including Dynamic Amplitude Dependence." Master's Thesis. Royal Institute of Technology, Stockholm, 2006.

Gil-Negrete, N., J. Vinolas, and L. Kari. "A Simplified Methodology to Predict the Dynamic Stiffness of Carbon-black Filled Rubber Isolators Using a Finite Element Code," *Journal of Sound and Vibration* 296 (2006): 757-76.

Kadlowec, J., A. Wineman, and G. Hulbert, "Elastomer Bushing Response: Experiments and Finite Element Modeling," Acta Mechanica, 163, 25-28, 2007.

Kim, S. and R. Singh, "Examination of High Frequency Characterization Methods for Mounts," SAE Transactions Journal of Passenger Cars: Mechanical Systems, (2002), 110(6), 1625-1633 (Paper # 2001-01-1444).

Lee, S. B. and A. Wineman, "A Model for Non-Linear Viscoelastic Axial Response of an Elastomeric Bushing," International Journal of Non-Linear Mechanics, 34, 779-793, 1999.

Lim, T.C., and R. Singh. “Vibration Transmission Through Rolling Element Bearings, Part I: Bearing Stiffness Formulation” *Journal of Sound and Vibration* (1990): **139**(2), 179-199.

MSC.Software, Inc., “Whitepaper - Nonlinear Finite Element Analysis of Elastomers,” 2010.

MTS Systems Corporation. *Accurate and Affordable Bushing Durability Test*. Web. 9 Mar. 2010. <http://www.mts.com/en/Material/Dynamic/index.asp>.

MTS Systems Corporation, Model 793.31 Dynamic Characterization Process – Operating Manual, 2000.

Piersol, A.G, T.L. Paez, and Harris, C.M.. *Harris’ Shock and Vibration Handbook, Sixth Edition,* Boston: McGraw-Hill, 2010.

Sohn, J.-H., S.-K. Lee, J.-K. Ok, and W.-S. Yoo. “Comparison of Semi-Physical and Black-Box Bushing Model for Vehicle Dynamics Simulation,” *Journal of Mechanical Science and Technology* 21 (2007): 264-71.

Stenti, A., D. Moens, P. Sas, and W. Desmet, “A Three-Level Non-Deterministic Modeling Methodology for the NVH Behavior of Rubber Connections,” Journal of Sound and Vibration, 329, 912-930, 2010.

Taulbee, R., “Estimation of Two-Dimensional Joint Stiffness Matrices Using Vibration Experiments,” Undergraduate Honors Thesis, Dept. of Mech. Eng., The Ohio State University, 2011.

Wolf, S., J. Haase, C. Claub, M. Jockel, and J. Losch, “Methods of Sensitivity Calculation Applied to a Multi-Axial Test Rig for Elastomer Bushings,” Thesis. Fraunhofer-Institute for Integrated Circuits, 2008.

Appendix A: List of Symbols

Symbols

K	spring stiffness [N/m]
L	distance between centers of spring and fixture [m]
r	vertical distance from pivot point to accelerometers [m]
O	pivot point
θ	rotation about pivot point [rad]
y	vertical displacement [m]
x	horizontal displacement [m]
M	reaction moment at pivot point [N-m]
R	reaction force at pivot point [N]
F	applied force [N]
δ	displacement [m]
ω	excitation frequency [rad/s]
ϕ	phase shift [rad]
I	Inertia of fixture about pivot point [$kg \cdot m^2$]
C	damping [N-m/rad/s]
α	adjustment factor

Subscripts

A	left of center
B	right of center
1	upper fixture
2	lower fixture
x	x-direction
y	y-direction
d	dynamic
T	torsional
n	natural

Superscripts

$\bar{}$ mean

$\sim$ harmonic

$*$ complex